Evaluation of PET imaging as a tool for detecting neonatal hypoxic-ischemic encephalopathy in a preclinical animal model

Saha, Emma; Shimochi, Saeka; Keller, Thomas; Eskola, Olli; López-Picón, Francisco; Rajander, Johan; Löyttyniemi, Eliisa; Forsback, Sarita; Solin, Olof; Grönroos, Tove J; Parikka, Vilhelmiina

Published in:
Experimental Neurology

DOI:
10.1016/j.expneurol.2023.114673

Published: 01/03/2024

Document Version
Final published version

Document License
CC BY

Experimental Neurology 373 (2024) 114673

Contents lists available at ScienceDirect

Experimental Neurology

journal homepage: www.elsevier.com/locate/yexnr

Research paper

Evaluation of PET imaging as a tool for detecting neonatal hypoxic-ischemic encephalopathy in a preclinical animal model

Emma Saha [a,b,c,*], Saeka Shimochi [a,b], Thomas Keller [d], Olli Eskola [d], Francisco López-Picón [a,b], Johan Rajander [e], Eliisa Löyttyniemi [f], Sarita Forsback [d], Olof Solin [d,e,g], Tove J. Grönroos [a,b,1], Vilhelmiina Parikka [a,b,c,h,1]

[a] Preclinical Imaging Laboratory, Turku PET Centre, University of Turku, Turku, Finland
[b] MediCity Research Laboratories, University of Turku, Turku, Finland
[c] Department of Pediatrics and Adolescent Medicine, Turku University Hospital, Turku, Finland
[d] Radiopharmaceutical Chemistry Laboratory, Turku PET Centre, University of Turku, Turku, Finland
[e] Accelerator Laboratory, Turku PET Centre, Åbo Akademi University, Turku, Finland
[f] Department of Biostatistics, University of Turku, Turku, Finland
[g] Department of Chemistry, University of Turku, Finland
[h] InFLAMES Research Flagship Center, University of Turku, Turku, Finland

ARTICLE INFO

Keywords:
Hypoxic-ischemic encephalopathy
Animal model
Brain injury
Neonatal
PET
Hypoxia
Inflammation
Energy metabolism

ABSTRACT

Hypoxic-ischemic encephalopathy due to insufficient oxygen delivery to brain tissue is a leading cause of death or severe morbidity in neonates. The early recognition of the most severely affected individuals remains a clinical challenge. We hypothesized that hypoxic-ischemic injury can be detected using PET radiotracers for hypoxia ([^{18}F]EF5), glucose metabolism ([^{18}F]FDG), and inflammation ([^{18}F]F-DPA).

Methods: A preclinical model of neonatal hypoxic-ischemic brain injury was made in 9-d-old rat pups by permanent ligation of the left common carotid artery followed by hypoxia (8% oxygen and 92% nitrogen) for 120 min. *In vivo* PET imaging was performed immediately after injury induction or at different timepoints up to 21 d later. After imaging, *ex vivo* brain autoradiography was performed. Brain sections were stained with cresyl violet to evaluate the extent of the brain injury and to correlate it with [^{18}F]FDG uptake.

Results: PET imaging revealed that all three of the radiotracers tested had significant uptake in the injured brain hemisphere. *Ex vivo* autoradiography revealed high [^{18}F]EF5 uptake in the hypoxic hemisphere immediately after the injury ($P < 0.0001$), decreasing to baseline even 1 d postinjury. [^{18}F]FDG uptake was highest in the injured hemisphere on the day of injury ($P < 0.0001$), whereas [^{18}F]F-DPA uptake was evident after 4 d ($P = 0.029$), peaking 7 d postinjury ($P < 0.0001$), and remained significant 21 d after the injury. Targeted evaluation demonstrated that [^{18}F]FDG uptake measured by *in vivo* imaging 1 d postinjury correlated positively with the brain volume loss detected 21 d later ($r = 0.72$, $P = 0.028$).

Conclusion: Neonatal hypoxic-ischemic brain injury can be detected using PET imaging. Different types of radiotracers illustrate distinct phases of hypoxic brain damage. PET may be a new useful technique, worthy of being explored for clinical use, to predict and evaluate the course of the injury.

1. Introduction

Hypoxic-ischemic encephalopathy (HIE) is the most severe birth complication related to perinatal oxygen deprivation. It originates from the lack of adequate blood flow and oxygen delivery to the brain within close temporal proximity to labor or birth. Neonatal HIE is a leading cause of death or severe morbidity in neonates occurring in 1–8 per 1000 live births in developed countries (Kurinczuk et al., 2010). Currently, therapeutic hypothermia remains the only therapeutic option for neonatal HIE, and it should be initiated within the first 6 h after birth (Jacobs et al., 2013; Wassink et al., 2019). Despite such treatment, there is a considerable burden of disability among surviving individuals. In

* Corresponding author at: University of Turku, MediCity/PET, Tykistökatu 6A, 4th floor, 20520 Turku, Finland.
E-mail address: emma.m.saha@utu.fi (E. Saha).
[1] Equal contribution.

https://doi.org/10.1016/j.expneurol.2023.114673
Received 13 September 2023; Received in revised form 9 December 2023; Accepted 29 December 2023
Available online 30 December 2023

addition, early recognition of the most severely affected individuals remains a clinical challenge (Murray, 2019; Walas et al., 2020).

In hypoxic-ischemic injury, the lack of sufficient oxygen and glucose delivery leads to a cascade where inflammation, excitotoxicity, and oxidative stress further exacerbate the tissue injury after the hypoxic-ischemic event (Gunn and Thoresen, 2019; Greco et al., 2020). The exact mechanisms behind this second phase of energy failure are not understood. Rapid reperfusion after the initial decrease in cerebral blood flow may further exacerbate the tissue injury.

The infant brain undergoes rapid and fundamental changes during the last weeks of gestation and the first postnatal months, thus making the developing brain unique and vulnerable to disruption (Dubois et al., 2014). Active growth, synaptogenesis, and myelination lead to increased metabolic demand for the brain tissue. Both cerebral blood flow (Tierradentro-García et al., 2021) and glucose consumption (Suhonen-Polvi et al., 1993; Shi et al., 2009; Odorcyk et al., 2020) increase rapidly with normal neurodevelopment after birth. Studies using PET imaging after neonatal hypoxic-ischemic brain injury are sparse. Both hypo- and hypermetabolism in the brain have been reported in preclinical (Odorcyk et al., 2020) and clinical (Suhonen-Polvi et al., 1993; Blennow et al., 1995; Shi et al., 2009) studies using the PET radiotracer [^{18}F]FDG.

This study tested the hypothesis that PET imaging can be used to characterize the impact of hypoxia ([^{18}F]EF5), glucose metabolism ([^{18}F]FDG), and neuroinflammation ([^{18}F]F-DPA) in different phases (0–21 d) after hypoxic-ischemic brain injury in a HIE rodent model. This was performed by *in vivo* imaging, *ex vivo* autoradiography, and immunohistochemistry. Our study provides new information about the cascade of biological mechanisms affecting brain injury development after neonatal HIE. This information may also be used for evaluating responses to new forms of treatment in preclinical models and could even lay the foundations for PET imaging of HIE neonates in the future.

2. Materials and methods

2.1. Study setup and HIE animal model

The study setup is illustrated in Fig. 1. Briefly, brain uptake of [^{18}F]EF5, [^{18}F]FDG, and [^{18}F]F-DPA was evaluated in control and HIE animals 0, 1, and 7 d after the injury. [^{18}F]F-DPA uptake was additionally evaluated on days 4 and 21. Tracer uptake was evaluated by *in vivo* imaging and *ex vivo* autoradiography. Studies were performed on healthy Spraque Dawley rat pups. All pups were kept with their dam at 21 ± 1.2 °C in 55 ± 5% humidity with a 12-h light/dark cycle at the Central Animal Laboratory, University of Turku, Turku, Finland. Dams had free access to tap water and food pellets. Both male and female pups were included in the study. The exact number of animals used, their ages and weights, as well as the injected doses and masses ([^{18}F]F-DPA only) for each study group and tracer are listed in Supplementary Table 1.

Neonatal HIE was induced using a widely recognized murine model in which brain injury results from a combination of unilateral ligation of the common carotid artery and systemic hypoxia (Fig. 1; Rice 3rd et al., 1981; Vannucci and Vannucci, 2005). Sprague-Dawley rat pups underwent ligation of the left common carotid artery under isoflurane anesthesia (4% isoflurane in oxygen for induction and 1.5–2% for maintenance) at postnatal days 9 or 10 (the age equivalent to the brain development of a term infant at birth). Subcutaneous buprenorphine was given for analgesia once before the operation. The ligation was performed from the neck incision with a silk suture after which the artery was permanently cut using electrocauterization. The animals were then returned to their dam for 1 h, whereafter they were exposed to systemic hypoxia for 2 h (8% O_2 and 92% N_2, P360 ProOx; BioSpherix) at a constant temperature (32 °C) to cause a unilateral hypoxic-ischemic brain injury. At this chamber temperature, the pup's body temperature remained at 36–37 °C as measured with a rectal thermometer. Sham controls underwent surgery without arterial ligation. Instead of hypoxic

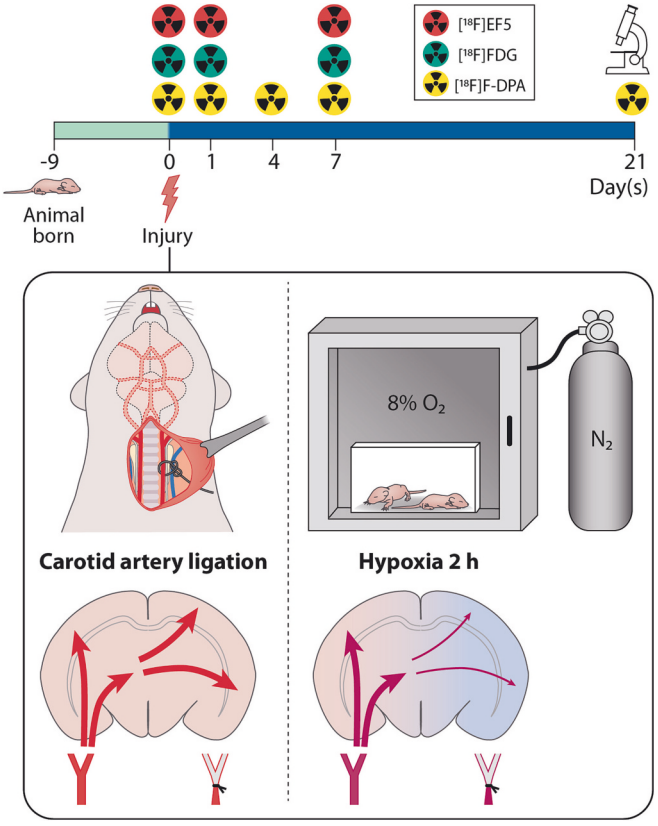

Fig. 1. Study setup. Schematic illustration of the experimental study design and preparation of the neonatal hypoxic-ischemic brain injury animal model. The left common carotid artery was permanently ligated and cut on postnatal day 9. After 1 h of recovery time, pups were exposed to hypoxia for 2 h. The uptake of [^{18}F]EF5, [^{18}F]FDG, and [^{18}F]F-DPA was evaluated in control and injured animals as a function of time using *in vivo* PET imaging and *ex vivo* autoradiography. The brain damage caused by the injury was evaluated 21 d later by immunohistochemical staining.

exposure, sham animals were kept at 36–37 °C in a cage, breathing normal room air, and isolated from their dam for 2 h. All animal experiments were approved by the Animal Experiment Board of the Province of Southern Finland (ESAVI/9611/2020) and carried out according to ARRIVE guidelines, the United Kingdom Animals (Scientific Procedures) Act 1986, and EU Directive 2010/63/EU for animal experiments.

2.2. Tracer radiosynthesis

[^{18}F]EF5 (2-(2-nitro-1H-imidazol-1-yl)-N-(2,2,3,3,3-[^{18}F]pentafluoropropyl)-acetamide) was synthesized as previously described (Eskola et al., 2012). The molar activity (A_m) of [^{18}F]EF5, decay-corrected to the end of synthesis (EOS), exceeded 3.7 GBq/μmol and the radiochemical purity exceeded 99%. [^{18}F]FDG (2-deoxy-2-[^{18}F]fluoro-D-glucose) was synthesized as described previously (Long et al., 2013), and the A_m at EOS was >100 GBq/μmol. Radiochemical purity exceeded 98%. [^{18}F]F-DPA ((N,N-diethyl-2-(2-(4-([^{18}F]fluoro)phenyl)-5,7-dimethylpyrazolo[1,5-*a*]pyrimidin-3-yl)acetamide)) was synthesized as previously described (Keller et al., 2017). The radiochemical purity exceeded 99% and the A_m at EOS exceeded 2 GBq/μmol.

2.3. PET/CT imaging and data analyses

Animals, 9–30 d old, weighing ~20–100 g on the study day were scanned with X- and β-cubes (Molecubes). Approximately 3–5 MBq (Supplementary Table 1) was injected intravenously under 2%

isoflurane anesthesia. The same animal was scanned in multiple timepoints or scanned only in one timepoint taking account of *ex vivo* analyses. Static scans were performed and reconstructed with an OSEM3D algorithm. Scan durations and initiations postinjection (p.i.) depended on the used tracer and are shown in Supplementary Table 2. A 10-min long CT scan was conducted before the PET scan.

The PMOD software (v. 4.0) was used to convert reconstructed DICOM images produced by the β-cube into an Inveon Research Workplace (v. 4.2) compatible DICOM format (Output SOP: PET IMAGE STORAGE or CT IMAGE STORAGE). For [^{18}F]EF5 analyses, standardized volumes of interest (VOIs) were placed over the whole injured hemisphere and related to whole brain uptake. For [^{18}F]FDG and [^{18}F]F-DPA analyses, VOIs were placed either in the whole hemisphere or in the following brain structures inside the hemisphere: hippocampus, cortex, striatum, and olfactory bulb. MRI age-matched templates were used as anatomic references (https://www.nitrc.org/frs/?group_id=669). Values were corrected for the injected dose and decay, and standardized uptake value $(SUV)_{mean}$ ratios were calculated for ipsilateral (injury)/contralateral (control) hemispheres (I/C ratio). For [^{18}F]FDG and [^{18}F]F-DPA analyses, I/C ratios were also calculated for each above-mentioned structure inside the hemisphere.

2.4. Ex vivo autoradiography

After the PET scan, the animals were sacrificed by cardiac puncture and transcardial perfusion. Brains were frozen in chilled isopentane and cut into 20-μm sections using a cryomicrotome (Leica CM3050) at four different brain levels (olfactory bulb, striatum, hippocampus, and cerebellum). The slides were exposed to an imaging plate (Fuji BAS Imaging Plate TR2025) for approximately 4 h and scanned using a Fuji BAS5000 analyzer. The ipsilateral-to-contralateral uptake ratio was calculated from the hippocampal level of injured animals at different timepoints. For regional brain analyses, regions of interest (ROIs) were drawn over the whole ipsilateral and contralateral hemispheres at the level of the olfactory bulb, striatum, and cerebellum. From the hippocampal level, three separate structures (cortex, hippocampus, and thalamus) were analyzed. These analyses were performed by calculating the structure-to-contralateral thalamus ratio for the ipsi- and contralateral hemispheres separately. The contralateral thalamus was used as an internal control area because of low tracer uptake. The results were calculated as photostimulated intensity/area − background (PSL/mm^2).

2.5. PK11195 pretreatment

To determine the specificity of [^{18}F]F-DPA uptake, 1 mg of the TSPO specific ligand PK11195 (ABX GmbH) was injected intraperitoneally into one injured (7 d earlier) animal 30 min before [^{18}F]F-DPA administration. The animal was sacrificed 40-min p.i., and the brain was sectioned for autoradiography analyses as described.

2.6. Immunohistochemistry staining

Brains were collected and fixed overnight in 10% formalin. Sections from the hippocampal brain level were immunohistochemically stained against Iba1 (microglia), GFAP (astrocytes), MAP2 (microtubule-associated protein-2), and NeuN (neurons) antigens. Antibodies used were Anti-Iba1 (1:2000; FUJIFILM Wako Pure Chemical Corporation Cat# 019–19,741), Anti-GFAP (1:100; Abcam Cat# ab4674), Anti-MAP2 (1:8000; Abcam Cat# ab183830), and Anti-NeuN (1:3000; Abcam Cat# ab177487).

2.7. Predictive value of [^{18}F]FDG

To study the predictive value of early [^{18}F]FDG uptake in the injured brain ($n = 9$), the brain volume loss was determined 21 d postinjury from brain sections stained with cresyl violet (Abcam Cat# ab246816). The area (mm^2) of volume loss in the injured brain hemisphere was determined as follows: (contralateral − ipsilateral hemisphere)/contralateral brain hemisphere × 100.

2.8. Statistical analysis

When the independent group means (either independent group data at the same study timepoint or different group of rats at different timepoints) were compared on continuous response, one-way analysis of variance (ANOVA) was used. After significant results, pairwise comparisons were made within the model and Dunnett pairwise correction was used, when applicable. If the same rats were measured over time, linear mixed models for repeated measurements were used. The model included group (between effect), timepoint (within effect), and group × time interaction. Pairwise comparisons between the groups and within-time comparisons were made in this model. A compound symmetry covariance structure was used. Some of the repeated measures models included only the time effect to determine whether a significant change occurred over timepoints separately for each brain region.

The Pearson correlation coefficient was calculated between two continuous variables to describe the strength of association. Additionally, the SUV ratio was compared between grouped severity of brain volume loss in the whole hemisphere and hippocampus using the Wilcoxon rank sum test. All data analyses were generated using SAS Version 9.4 of the SAS System for Windows (SAS Institute Inc.).

3. Results

3.1. In vivo PET imaging

The hypoxic-ischemic injury resulted in decreased animal growth compared to sham-operated pups (Supplementary Fig. 1). All three radiotracers revealed increased SUV_{mean} I/C ratios either on the injury day or at later timepoints (Fig. 2A). Administration of [^{18}F]EF5 immediately before the hypoxic exposure led to significantly ($P < 0.0001$; Supplementary Fig. 2) increased tracer uptake in the injured hemisphere compared to the whole brain. Since [^{18}F]EF5 uptake was homogenous in the injured hemisphere, and only visible at the injury day, a detailed regional brain analysis was not performed. The highest [^{18}F]FDG SUV_{mean} I/C ratios were seen on the injury day (Fig. 2B). This uptake declined significantly already 1 d later and remained similar 7 d later. Regional brain analysis revealed significantly higher [^{18}F]FDG SUV_{mean} I/C ratios in hippocampus, cortex, and striatum at the injury day compared to later timepoints. The increased uptake in the area of the olfactory bulb occurred to a lesser extent. [^{18}F]F-DPA SUV_{mean} I/C ratios were not significantly different in the injured hemisphere 1 d after the injury, but were significantly increased 4 d later in hippocampal, cortical, and striatal areas (Fig. 2B). This uptake peaked at 7 d postinjury and was detectable as late as 21 d after the injury.

3.2. Ex vivo brain autoradiography

Fig. 3A illustrates the uptake pattern of [^{18}F]EF5, [^{18}F]FDG, and [^{18}F]F-DPA as a function of time in control and injured animals at the hippocampal brain level, as shown in hematoxylin and eosin (H&E)-stained images. [^{18}F]EF5 uptake was significantly higher ($P < 0.0001$) and quite homogenously distributed in the injured hemisphere when injected before the hypoxic exposure. In 2 of 8 animals, uptake infiltrated into the contralateral hemisphere (Supplementary Fig. 3B). Furthermore, if [^{18}F]EF5 was injected immediately after the hypoxia exposure, the uptake pattern changed and was detected only in a smaller cortical area in the injured hemisphere (Supplementary Fig. 3C and 3D). At later timepoints, 1–7 d after the injury, there was no detectable [^{18}F]EF5 uptake (Fig. 3). Similar to the *in vivo* imaging findings, the highest [^{18}F]FDG uptake was found in the injured hemisphere ($P < 0.0001$) on the day of injury (Fig. 3). [^{18}F]F-DPA uptake was evident on day 4 ($P =$

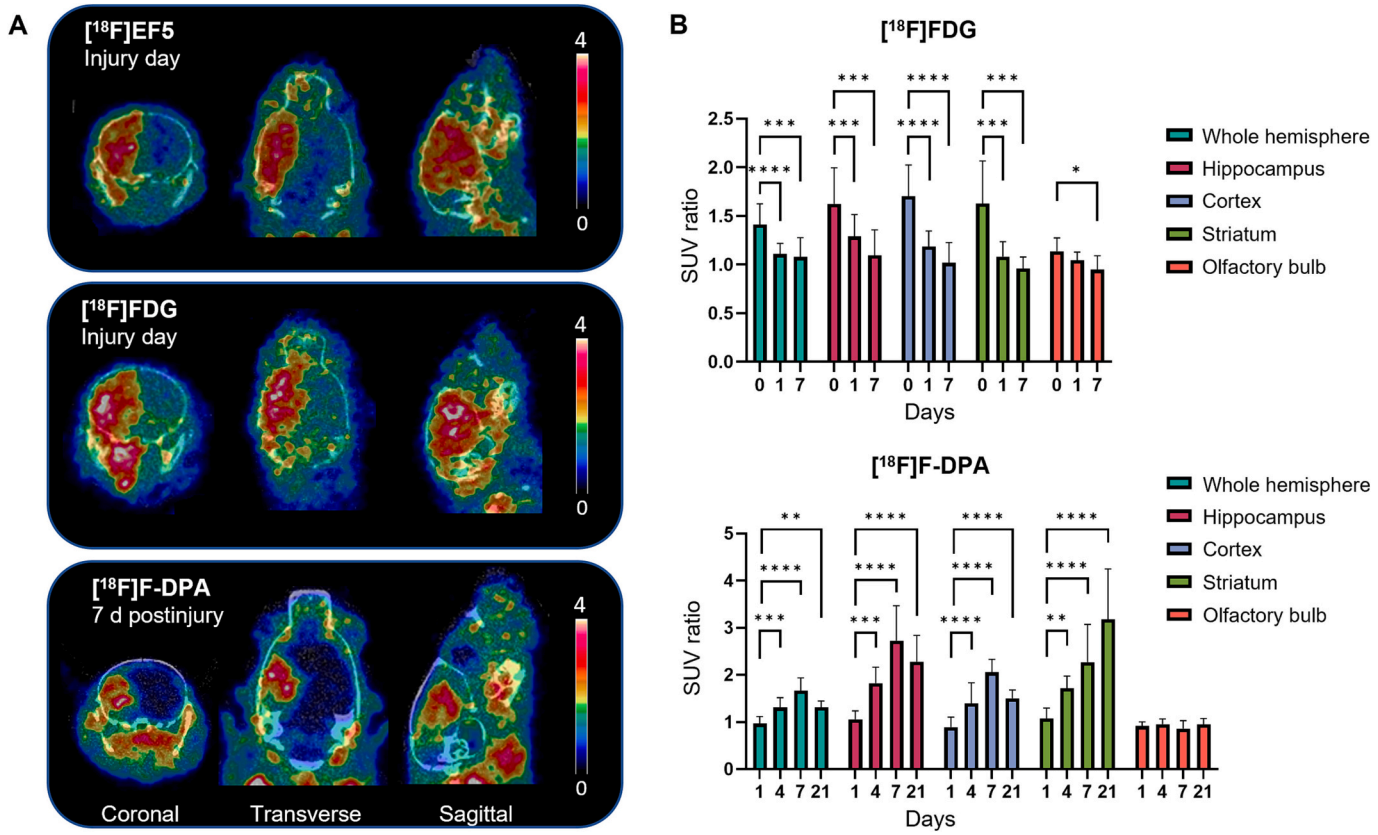

Fig. 2. *In vivo* PET imaging. (A) PET/CT images demonstrating [^{18}F]EF5, [^{18}F]FDG, and [^{18}F]F-DPA uptake expressed as SUV_{mean} values in an injured brain from coronal, transverse, and sagittal planes. (B) SUV_{mean} uptake ratios of different brain regions for [^{18}F]FDG (0–7 d after injury) and [^{18}F]F-DPA (1–21 d after injury). Data are expressed as ipsilateral/contralateral ratio. For [^{18}F]FDG analyses n = 5–12/group and for [^{18}F]F-DPA n = 5–14/group. *$P < 0.05$, **$P < 0.01$, ***$P < 0.001$, ****$P < 0.0001$.

0.029) and peaked 7 d ($P < 0.0001$) postinjury in the ipsilateral hemisphere. This uptake was still evident at 21 d ($P = 0.0005$) after the brain injury (Fig. 3).

To further evaluate the uptake pattern of the tracers in different brain areas, analyses were performed at four separate brain levels (Fig. 4A). These analyses were done on the injury day for [^{18}F]EF5 and [^{18}F]FDG and 7 d after the injury for [^{18}F]F-DPA, *i.e.*, timepoints showing the highest individual tracer uptake. Regional brain areas that were analyzed are shown in the H&E-stained images in Fig. 4A.

Significantly higher [^{18}F]EF5 uptake was detected in the olfactory bulb ($P = 0.0009$), striatum ($P < 0.0001$), cortex ($P = 0.008$), hippocampus ($P < 0.0001$), and thalamus ($P < 0.0001$) on the injury day (Fig. 4B). [^{18}F]FDG showed a more heterogeneous uptake profile in the brain regions and was significantly increased in the olfactory bulb ($P = 0.043$), striatum ($P = 0.038$), hippocampus ($P = 0.028$), and thalamus ($P = 0.031$). Cortical uptake varied considerably and did not reach significance, whereas the cerebellum remained unaffected. [^{18}F]F-DPA uptake was also heterogeneously distributed inside the ipsilateral hemisphere and was most prominent in the cortical ($P = 0.001$) and hippocampal ($P = 0.035$) areas. The major variation among individuals was detected in these areas, showing increased I/C ratios ranging from 4-fold to 25-fold. No specific [^{18}F]F-DPA uptake was seen in the cerebellum.

3.3. PK11195 pretreatment

Pretreatment with PK11195 before the injection of [^{18}F]F-DPA completely inhibited tracer uptake in the injured hemisphere, as determined by autoradiography analyses (Supplementary Fig. 4).

3.4. Immunohistochemistry

Changes after HIE brain injury were also assessed by immunohistochemistry. Increased microgliosis and astrogliosis in the injured hemisphere were detected with Iba-1 and GFAP antibodies, respectively. MAP-2 and NeuN immunostaining revealed neuronal loss and cortical thinning in the injured hemisphere (Fig. 5).

3.5. Prognostic value of [^{18}F]FDG

[^{18}F]FDG uptake, measured by *in vivo* imaging 1 d postinjury, correlated with the brain volume loss detected 21 d later (Fig. 6A and B). Pearson's correlation analysis revealed a correlation between brain volume loss and [^{18}F]FDG uptake in the ipsilateral hemisphere ($r = 0.72$, $P = 0.028$) and the hippocampal area ($r = 0.75$, $P = 0.021$). Similar, albeit not significant, results were achieved when animals were grouped by the severity of brain volume loss (cutoff 30%) (Fig. 6C).

4. Discussion

We have demonstrated that PET imaging can be used to detect neonatal HIE and to measure injury severity in the acute phase of brain injury. Imaging findings were highly dependent on timing. The uptake of [^{18}F]EF5 (hypoxia), [^{18}F]FDG (glucose metabolism), and [^{18}F]F-DPA (inflammation) reflected distinct phases, affecting different substructural brain regions, during injury progression.

PET imaging was useful for the early detection of hypoxia. On the injury day, [^{18}F]EF5 uptake showed a uniform distribution in the whole ipsilateral hemisphere, which proved the functionality of the biological mechanism leading to brain injury in this animal model. This uptake was

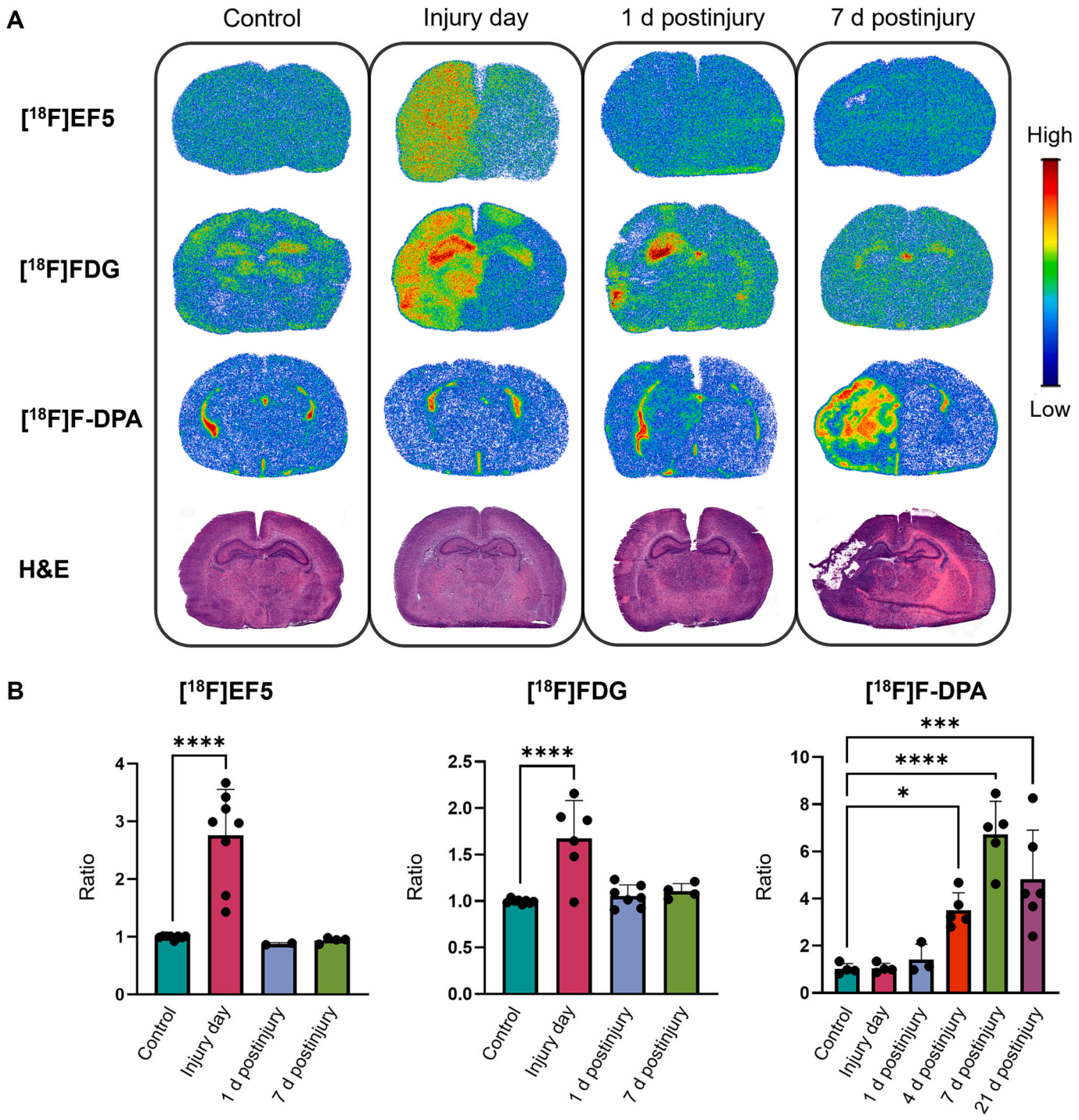

Fig. 3. *Ex vivo* brain autoradiography from the hippocampal level. (A) Representative autoradiography images of brain sections from control and injured animals showing the uptake pattern of [^{18}F]EF5, [^{18}F]FDG, and [^{18}F]F-DPA at different timepoints at the hippocampal level. H&*E*-stained sections illustrating the brain level used for the analyses. (B) The ipsilateral-to-contralateral uptake ratio was calculated on the injury day and postinjury days 1 and 7. For [^{18}F]F-DPA, the ratios were also calculated for postinjury days 4 and 21. Data are expressed as mean ± SD of photostimulated intensity per area − background (PSL/mm^2). For [^{18}F]EF5 n = 2–8/group, [^{18}F]FDG n = 4–8/group, [^{18}F]F-DPA n = 3–6/group. *P < 0.05, ***P < 0.001, ****P < 0.0001.

focused on a smaller cortical area if EF5 was injected after initiation of the hypoxic exposure. This finding is in line with previous studies using [^{18}F]FMISO, where hypoxic brain areas were detected in the affected cortex in an adult rodent model of ischemic stroke (Takasawa et al., 2007; Williamson et al., 2013). The smaller cortical area detected with [^{18}F]EF5 was in line with the location of the injury, as determined by histopathological analysis three weeks later.

A few studies using [^{18}F]FDG in experimental HIE models have previously been reported. Decreased [^{18}F]FDG uptake in the injured area was reported at postnatal day 27–29 in a hybrid animal model combining systemic inflammation (lipopolysaccharide injection) and hypoxic-ischemic brain injury (Chevin et al., 2020). Odorcyk et al. (2020) demonstrated decreased [^{18}F]FDG uptake in the lesion area 72 h postinjury. To our knowledge, [^{18}F]FDG uptake has not previously been investigated immediately after the injury. The increased [^{18}F]FDG uptake in brain regions, especially the hippocampus, and the cortex, of the

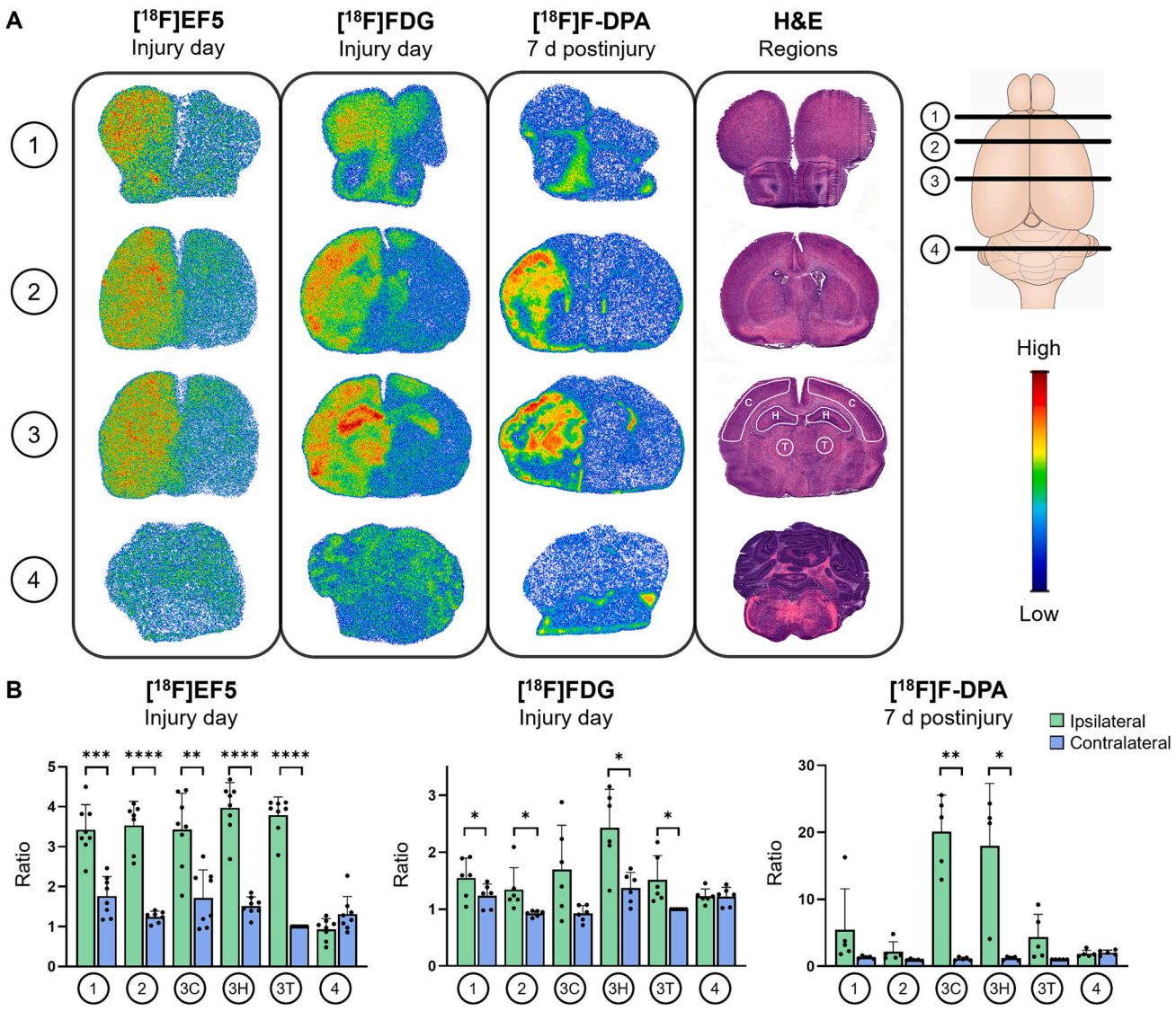

Fig. 4. *Ex vivo* brain autoradiography from four different brain levels. (A) Representative autoradiography images illustrating the uptake pattern of [^{18}F]EF5, [^{18}F]FDG, and [^{18}F]F-DPA at four different brain levels: 1 = olfactory bulb, 2 = striatum, 3 = hippocampus (including cortex [3C], hippocampus [3H], and thalamus [3T] separately), and 4 = cerebellum. For each tracer, the timepoint after the injury showing maximal tracer uptake was selected. H&E-stained sections showing the brain regions used for the analyses. (B) For levels 1, 2, and 4, ROIs were drawn over the whole ipsilateral and contralalteral hemispheres. For level 3, ROIs were drawn over the cortex, hippocampus, and thalamus. The structure-to-contralateral thalamus (PSL/mm^2) ratio was calculated for both hemispheres separately, resulting in a ratio of 1 for the contralateral thalamus. For [^{18}F]EF5 $n = 8$, [^{18}F]FDG $n = 6$, [^{18}F]F-DPA $n = 5$. *$P < 0.05$, **$P < 0.01$, ***$P < 0.001$, ****$P < 0.0001$.

ipsilateral hemisphere was evident in our animal model. This uptake is likely associated with an activated reperfusion phase, known to happen due to the Circle of Willis also in injured animals, and compensation for reduced oxidative phosphorylation due to hypoxia. At later timepoints (1–3 d), the increased energy metabolism was less evident, although slightly increased [^{18}F]FDG uptake was still seen in the hippocampus. Both glucose hypo- and hypermetabolism have previously been reported in experimental animal models mimicking hypoxic-ischemic brain injury in adults after cardiac arrest (Kim et al., 2019; Zhang et al., 2021; Bajorat et al., 2022).

Some pilot-type PET studies have been conducted in clinical settings with infants at various timepoints (days to months) after HIE injury, revealing both glucose hypo- (Suhonen-Polvi et al., 1993) and hypermetabolism (Blennow et al., 1995). In addition, one case report using [^{18}F]FDG imaging reported that transient glucose hypermetabolism in the basal ganglia was replaced by severe glucose hypometabolism four years later (Batista et al., 2007). Our data is in accordance with the hypothesis that transient hypermetabolism occurs in damaged brain regions in the acute phase of HIE injury (Chugani, 2021). This finding has not been systematically reported in previous studies since most studies were conducted in a later, subacute, or chronic state.

As new whole-body PET/CT scanners enable very short scan sessions, with increased sensitivity and significantly lower radiation doses (Slart et al., 2021), we consider PET imaging as a potential diagnostic tool to determine the severity of brain injuries in newborn HIE patients in the future. Before that, some logistic challenges remain to be carefully evaluated as *e.g.* safe transfer of the HIE infant to a PET department, choosing the most predictable tracer and time point for the scan. Hence, we determined the predictive value of [^{18}F]FDG uptake as detected by *in vivo* imaging 1 d postinjury. Indeed, our results show that uptake correlates with brain volume loss, as determined by immunohistochemical evaluation 21 d later. Contradictorily to our finding, decreased [^{18}F]FDG uptake, determined 72 h post injury, predicted impaired cognition and a worse outcome in an animal model (Odorcyk et al., 2020). We posit that both scenarios are of prognostic value: glucose hypermetabolism in the early injury phase and hypometabolism in the later phase.

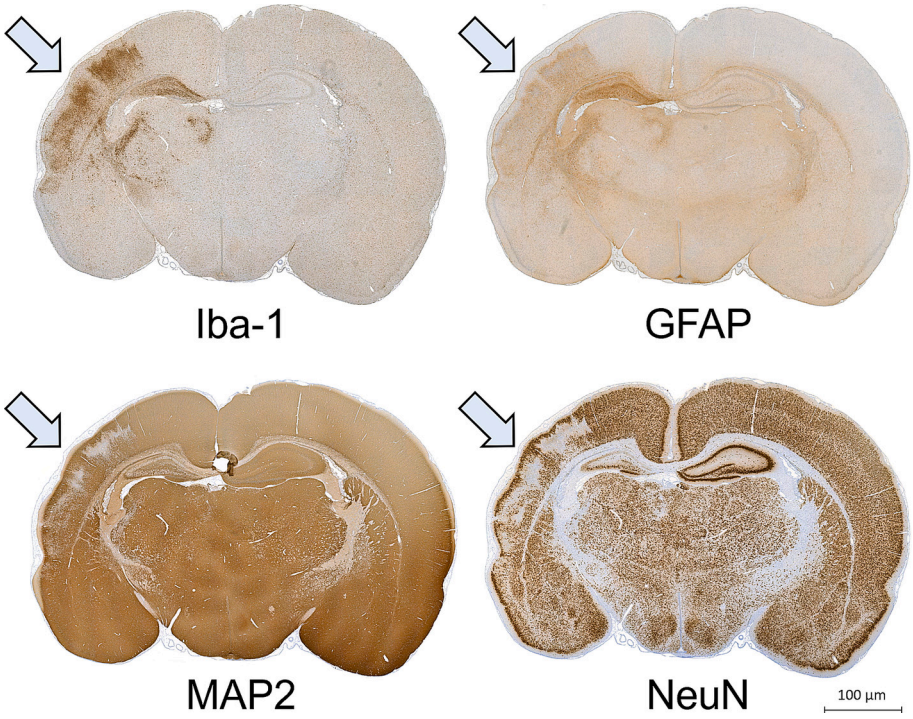

Fig. 5. Immunohistochemistry. Immunohistochemical staining against Iba-1 (microglia), GFAP (astrocytes), MAP-2 (microtubules), and NeuN (neurons) antigens in the brains of HIE rats 7 d after injury. Arrows indicate areas of damage.

Further studies are needed to investigate the role of glucose metabolism during HIE injury development as a function of time. Differences in regional [^{18}F]FDG uptake may be of particular interest when using PET as a tool to provide prognostic information (Kim et al., 2019). Our data indicate that hippocampal [^{18}F]FDG SUV ratios have the best capability to distinguish more severely injured animals from less injured ones.

Increased [^{18}F]F-DPA uptake in the injured hemisphere was evident on day 4, peaked on day 7, and remained detectable 21 d after the injury. In a previous study, [^{18}F]GE180 failed to detect a cerebral inflammatory response caused by severe asphyxia in newborn piglets in the early phase (within 32 h) after global hypoxia (de Lange et al., 2018). To our knowledge, this is the first study demonstrating the utility of PET imaging in visualising and quantifying inflammatory responses in HIE. Our results are consistent with previous studies performed with preclinical stroke models, reporting an increased TSPO tracer uptake later (14–16 d) postinjury (Wang et al., 2014; Tóth et al., 2016). Blocking with PK11195 totally inhibited [^{18}F]F-DPA brain uptake. Our results are in line with a previously reported recommendation that TSPO-PET tracers are useful for imaging neuroinflammation 3–7 d post injury (Dickens et al., 2014).

This study has limitations. First, the neonatal hypoxic-ischemic brain injury model used in this study does not mimic all aspects of clinical brain injury. The resulting brain injury in this animal model is unilateral and thus not identical to the injury occurring in a newborn. However, the model is well-established and widely used to study the pathophysiological processes of neonatal hypoxic-ischemic injury and to test different therapy concepts (Vannucci and Vannucci, 2005; Hamdy et al., 2020). Furthermore, we consider the basic pathophysiological processes to be similar in the HIE injury animal model and the clinical situation. Thus, we consider this model as the best available choice. Second, the predictive prognostic value of [^{18}F]FDG reported in this study is based on rough estimation and must be evaluated in more detail and at different timepoints in future studies. Although [^{18}F]FDG is probably the most potent candidate for prognostic clinical studies, due to its wide availability and capability to detect early metabolic changes, our results also support future studies to evaluate the predictive value of other PET tracers.

5. Conclusion

PET imaging is feasible in a HIE injury animal model in young pups. We showed the usefulness of [^{18}F]EF5, [^{18}F]FDG, and [^{18}F]F-DPA to detect different pathophysiological events of hypoxic-ischemic injury in brain tissue. Our results demonstrate that [^{18}F]FDG uptake a day after the injury correlates with the severity of the histopathological brain injury three weeks later, indicating that PET imaging may be a promising tool to predict neurological outcomes in neonatal hypoxic-ischemic injury even in clinical settings. [^{18}F]FDG and [^{18}F]F-DPA animal imaging studies may not only be used to further evaluate new treatment options for HIE, but also to further investigate the pathophysiological processes that evolve after HIE injury.

Funding

This research was supported by the InFLAMES Flagship Programme of the Academy of Finland [337530]; Foundation for Pediatric Research, Finland [190154, 210225, and 210186]; The South-Western Finnish Foundation of Neonatal Research; The Finnish Cultural Foundation (Varsinais-Suomi Regional Fund); Päivikki and Sakari Sohlberg Foundation; The State Funding for University Level Health Research in Finland (Turku University Hospital); and The Finnish Medical Foundation [5159]. The authors declare no conflict of interest.

Author contributions

Emma Saha, Tove Grönroos, and Vilhelmiina Parikka designed the experiments, participated in the data collection and interpretation, and were responsible for writing the manuscript. Material preparation and data collection were performed by Saeka Shimochi, Johan Rajander, Thomas Keller, Olli Eskola, Sarita Forsback, Olof Solin, and Francisco López-Picón. Eliisa Löyttyniemi carried out statistical analyses. All authors read and approved the final manuscript.

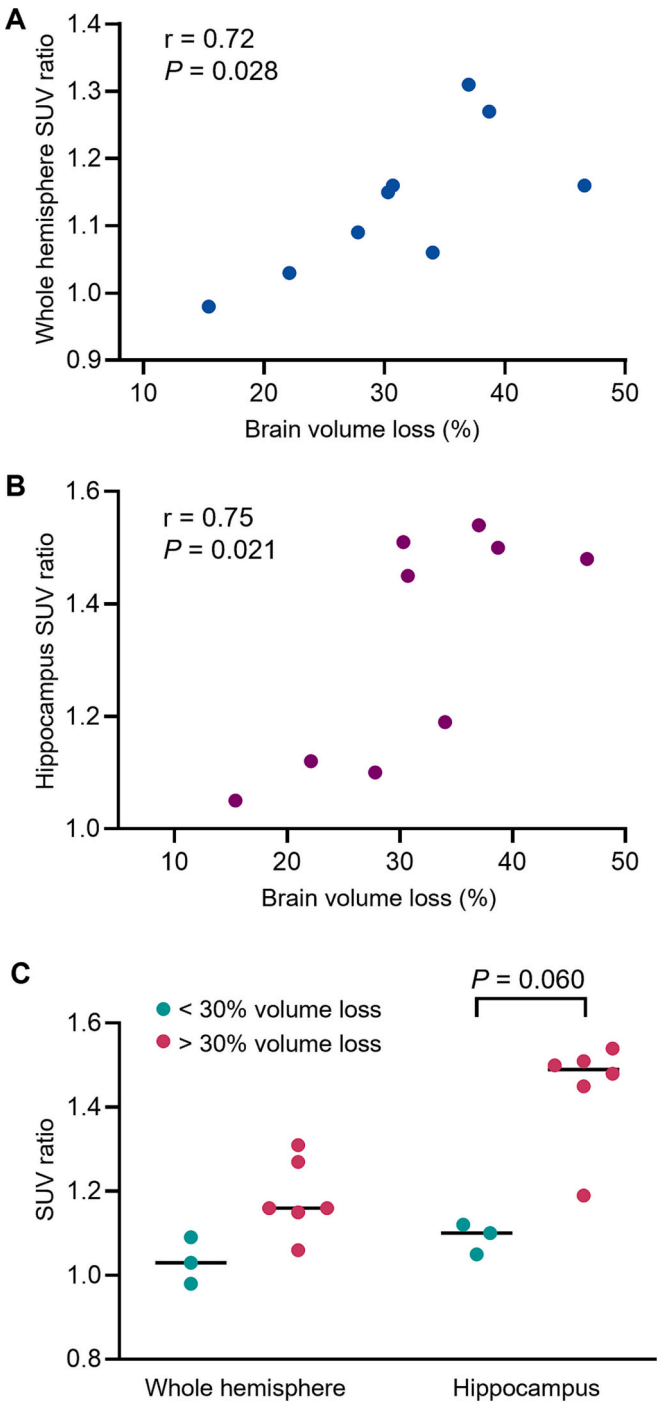

Fig. 6. Prognostic value of [^{18}F]FDG. Pearson correlations between the individual brain volume loss and [^{18}F]FDG SUV ratios (1 d after injury) for (A) the ipsilateral hemisphere and (B) the hippocampus inside the ipsilateral hemisphere revealed a prognostic value of [^{18}F]FDG uptake (n = 9). (C) The hippocampal area also showed clearly higher [^{18}F]FDG SUV ratios between the ipsilateral and contralateral hemispheres (P = 0.060) when the animals were divided by a cutoff of 30% in brain volume loss.

CRediT authorship contribution statement

Emma Saha: Conceptualization, Methodology, Validation, Formal analysis, Investigation, Data curation, Writing – original draft, Visualization. **Saeka Shimochi:** Methodology, Investigation, Data curation, Writing – review & editing. **Thomas Keller:** Methodology, Investigation, Writing – review & editing. **Olli Eskola:** Methodology, Resources, Writing – review & editing. **Francisco López-Picón:** Methodology, Investigation, Writing – review & editing. **Johan Rajander:** Methodology, Resources. **Eliisa Löyttyniemi:** Formal analysis, Data curation, Writing – original draft. **Sarita Forsback:** Methodology, Resources, Writing – review & editing. **Olof Solin:** Methodology, Resources, Writing – review & editing. **Tove J. Grönroos:** Conceptualization, Methodology, Validation, Investigation, Writing – original draft, Visualization, Supervision, Project administration. **Vilhelmiina Parikka:** Conceptualization, Methodology, Validation, Investigation, Writing – original draft, Visualization, Supervision, Project administration, Funding acquisition.

Declaration of competing interest

The authors declare that they have no known competing financial interests or personal relationships that could have appeared to influence the work reported in this paper.

Data availability

Analyzed datasets are available from the corresponding author on reasonable request.

Acknowledgments

We acknowledge the Preclinical Imaging Laboratory and Accelerator Laboratory personnel, as well as the staff of Central Animal Laboratory of the University of Turku. We acknowledge Joe Hettinger for the linguistic editing of the manuscript. The histological methods were performed by the Histology Core Facility of the Institute of Biomedicine, University of Turku.

Appendix A. Supplementary data

Supplementary data to this article can be found online at https://doi.org/10.1016/j.expneurol.2023.114673.

References

Bajorat, R., Kurth, J., Stenzel, J., et al., 2022. Early post-ischemic brain glucose metabolism is dependent on function of TLR2: a study using [^{18}F]F-FDG PET-CT in a mouse model of cardiac arrest and cardiopulmonary resuscitation. Mol. Imaging Biol. 24, 466–478. https://doi.org/10.1007/s11307-021-01677-y.

Batista, C.E., Chugani, H.T., Juhász, C., Behen, M.E., Shankaran, S., 2007. Transient hypermetabolism of the basal ganglia following perinatal hypoxia. Pediatr. Neurol. 36, 330–333. https://doi.org/10.1016/j.pediatrneurol.2007.01.004.

Blennow, M., Ingvar, M., Lagercrantz, H., et al., 1995. Early [^{18}F]FDG positron emission tomography in infants with hypoxic-ischaemic encephalopathy shows hypermetabolism during the postasphyctic period. Acta Paediatr. 84, 1289–1295. https://doi.org/10.1111/j.1651-2227.1995.tb13551.x.

Chevin, M., Chabrier, S., Dinomais, M., Bedell, B.J., Sébire, G., 2020. Benefits of hypothermia in neonatal arterial ischemic strokes: a preclinical study. Int. J. Dev. Neurosci. 80, 257–266. https://doi.org/10.1002/jdn.10022.

Chugani, H.T., 2021. Hypermetabolism on pediatric PET scans of brain glucose metabolism: what does it signify? J. Nucl. Med. 62, 1301–1306. https://doi.org/10.2967/jnumed.120.256081.

de Lange, C., Solberg, R., Holtedahl, J.E., et al., 2018. Dynamic TSPO-PET for assessing early effects of cerebral hypoxia and resuscitation in new born pigs. Nucl. Med. Biol. 66, 49–57. https://doi.org/10.1016/j.nucmedbio.2018.08.004.

Dickens, A.M., Vainio, S., Marjamäki, P., et al., 2014. Detection of microglial activation in an acute model of neuroinflammation using PET and radiotracers 11C-(R)-PK11195 and 18F-GE-180. J. Nucl. Med. 55, 466–472. https://doi.org/10.2967/jnumed.113.125625.

Dubois, J., Dehaene-Lambertz, G., Kulikova, S., Poupon, C., Hüppi, P.S., Hertz-Pannier, L., 2014. The early development of brain white matter: a review of imaging studies in fetuses, newborns and infants. Neuroscience. 276, 48–71. https://doi.org/10.1016/j.neuroscience.2013.12.044.

Eskola, O., Grönroos, T.J., Forsback, S., et al., 2012. Tracer level electrophilic synthesis and pharmacokinetics of the hypoxia tracer [^{18}F]EF5. Mol. Imaging Biol. 14, 205–212. https://doi.org/10.1007/s11307-011-0484-4.

Greco, P., Nencini, G., Piva, I., et al., 2020. Pathophysiology of hypoxic-ischemic encephalopathy: a review of the past and a view on the future. Acta Neurol. Belg. 120, 277–288. https://doi.org/10.1007/s13760-020-01308-3.

Gunn, A.J., Thoresen, M., 2019. Neonatal encephalopathy and hypoxic-ischemic encephalopathy. Handb. Clin. Neurol. 162, 217–237. https://doi.org/10.1016/B978-0-444-64029-1.00010-2.

Hamdy, N., Eide, S., Sun, H.S., Feng, Z.P., 2020. Animal models for neonatal brain injury induced by hypoxic ischemic conditions in rodents. Exp. Neurol. 334, 113457 https://doi.org/10.1016/j.expneurol.2020.113457.

Jacobs, S.E., Berg, M., Hunt, R., Tarnow-Mordi, W.O., Inder, T.E., Davis, P.G., 2013. Cooling for newborns with hypoxic ischaemic encephalopathy. Cochrane Database Syst. Rev. 1, CD00331. https://doi.org/10.1002/14651858.CD003311.pub3.

Keller, T., Krzyczmonik, A., Forsback, S., et al., 2017. Radiosynthesis and preclinical evaluation of [^{18}F]F-DPA, a novel pyrazolo [1,5a]pyrimidine acetamide TSPO radioligand, in healthy Sprague Dawley rats. Mol. Imaging Biol. 19, 736–745. https://doi.org/10.1007/s11307-016-1040-z.

Kim, D., Yoon, H.J., Lee, W.J., Woo, S.H., Kim, B.S., 2019. Prognostic value of ^{18}F-FDG brain PET as an early indicator of neurological outcomes in a rat model of post-cardiac arrest syndrome. Sci. Rep. 9, 14798. https://doi.org/10.1038/s41598-019-51327-1.

Kurinczuk, J.J., White-Koning, M., Badawi, N., 2010. Epidemiology of neonatal encephalopathy and hypoxic-ischaemic encephalopathy. Early Hum. Dev. 86, 329–338. https://doi.org/10.1016/j.earlhumdev.2010.05.010.

Long, J.Z., Jacobson, M.S., Hung, J.C., 2013. Comparison of FASTlab [18^{F}]FDG production using phosphate and citrate buffer cassettes. J. Nucl. Med. Technol. 41, 32–34. https://doi.org/10.2967/jnmt.112.112649.

Murray, D.M., 2019. Biomarkers in neonatal hypoxic-ischemic encephalopathy-review of the literature to date and future directions for research. Handb. Clin. Neurol. 162, 281–293. https://doi.org/10.1016/B978-0-444-64029-1.00013-8.

Odorcyk, F.K., Duran-Carabali, L.E., Rocha, D.S., et al., 2020. Differential glucose and beta-hydroxybutyrate metabolism confers an intrinsic neuroprotection to the immature brain in a rat model of neonatal hypoxia ischemia. Exp. Neurol. 330, 113317 https://doi.org/10.1016/j.expneurol.2020.113317.

Rice 3rd, J.E., Vannucci, R.C., Brierley, J.B., 1981. The influence of immaturity on hypoxic-ischemic brain damage in the rat. Ann. Neurol. 9, 131–141. https://doi.org/10.1002/ana.410090206.

Shi, Y., Jin, R.B., Zhao, J.N., Tang, S.F., Li, H.Q., Li, T.Y., 2009. Brain positron emission tomography in preterm and term newborn infants. Early Hum. Dev. 85, 429–432. https://doi.org/10.1016/j.earlhumdev.2009.02.002.

Slart, R.H.J.A., Tsoumpas, C., Glaudemans, A.W.J.M., Noordzij, W., Willemsen, A.T.M., Borra, R.J.H., et al., 2021. Long axial field of view PET scanners: a road map to implementation and new possibilities. Eur. J. Nucl. Med. Mol. Imaging 48 (13), 4236–4245. https://doi.org/10.1007/s00259-021-05461-6.

Suhonen-Polvi, H., Kero, P., Korvenranta, H., et al., 1993. Repeated fluorodeoxyglucose positron emission tomography of the brain in infants with suspected hypoxic-ischaemic brain injury. Eur. J. Nucl. Med. 20, 759–765. https://doi.org/10.1007/BF00180905.

Takasawa, M., Beech, J.S., Fryer, T.D., et al., 2007. Imaging of brain hypoxia in permanent and temporary middle cerebral artery occlusion in the rat using 18F-fluoromisonidazole and positron emission tomography: a pilot study. J. Cereb. Blood Flow Metab. 27, 679–689. https://doi.org/10.1038/sj.jcbfm.9600405.

Tierradentro-García, L.O., Saade-Lemus, S., Freeman, C., et al., 2021 Jul 5. Cerebral blood flow of the neonatal brain after hypoxic-ischemic injury. Am. J. Perinatol. https://doi.org/10.1055/s-0041-1731278.

Tóth, M., Little, P., Arnberg, F., et al., 2016. Acute neuroinflammation in a clinically relevant focal cortical ischemic stroke model in rat: longitudinal positron emission tomography and immunofluorescent tracking. Brain Struct. Funct. 221, 1279–1290. https://doi.org/10.1007/s00429-014-0970-y.

Vannucci, R.C., Vannucci, S.J., 2005. Perinatal hypoxic-ischemic brain damage: evolution of an animal model. Dev. Neurosci. 27, 81–86. https://doi.org/10.1159/000085978.

Walas, W., Wilińska, M., Bekiesińska-Figatowska, M., Halaba, Z., Śmigiel, R., 2020. Methods for assessing the severity of perinatal asphyxia and early prognostic tools in neonates with hypoxic-ischemic encephalopathy treated with therapeutic hypothermia. Adv. Clin. Exp. Med. 29, 1011–1016. https://doi.org/10.17219/acem/124437.

Wang, Y., Yue, X., Kiesewetter, D.O., et al., 2014. [^{18}F]DPA-714 PET imaging of AMD3100 treatment in a mouse model of stroke. Mol. Pharm. 11, 3463–3470. https://doi.org/10.1021/mp500234d.

Wassink, G., Davidson, J.O., Dhillon, S.K., et al., 2019. Therapeutic hypothermia in neonatal hypoxic-ischemic encephalopathy. Curr. Neurol. Neurosci. Rep. 19, 2. https://doi.org/10.1007/s11910-019-0916-0.

Williamson, D.J., Ejaz, S., Sitnikov, S., et al., 2013. A comparison of four PET tracers for brain hypoxia mapping in a rodent model of stroke. Nucl. Med. Biol. 40, 338–344. https://doi.org/10.1016/j.nucmedbio.2012.11.012.

Zhang, H.J., Mitchell, S., Fang, Y.H., et al., 2021. Assessment of brain glucose metabolism following cardiac arrest by [^{18}F]FDG positron emission tomography. Neurocrit. Care. 34, 64–72. https://doi.org/10.1007/s12028-020-00984-6.